In the format provided by the authors and unedited.

Structures of capsid and capsid-associated tegument complex inside the Epstein–Barr virus

Wei Liu[1,2,3,8], Yanxiang Cui [1,8], Caiyan Wang[1,2,4], Zihang Li [1,2], Danyang Gong[5,6], Xinghong Dai[1,2,7], Guo-Qiang Bi [3], Ren Sun[1,5] and Z. Hong Zhou [1,2] ✉

[1]California NanoSystems Institute, University of California, Los Angeles, Los Angeles, CA, USA. [2]Department of Microbiology Immunology and Molecular Genetics, University of California, Los Angeles, Los Angeles, CA, USA. [3]Center for Integrative Imaging, Hefei National Laboratory for Physical Sciences at the Microscale, and School of Life Sciences, University of Science and Technology of China, Hefei, China. [4]International Institute for Translational Chinese Medicine, Guangzhou University of Chinese Medicine, Guangzhou, China. [5]Department of Molecular and Medical Pharmacology, University of California, Los Angeles, Los Angeles, CA, USA. [6]Present address: Department of Therapeutics Discovery, Amgen Research, Amgen Inc., Thousand Oaks, CA, USA. [7]Present address: Department of Physiology and Biophysics, School of Medicine, Case Western Reserve University, Cleveland, OH, USA. [8]These authors contributed equally: Wei Liu, Yanxiang Cui. ✉e-mail: Hong.Zhou@ucla.edu

Supporting Information

Structures of Capsid and Capsid-Associated Tegument Complex inside the Epstein-Barr Virus

Wei Liu, Yanxiang Cui *et al*.

List of Content

Supplementary Discussion

Inter-MCP interactions and structural plasticity of the 20 MCP conformers

First recognized in HCMV[1] and subsequently confirmed in HSV[2-4], HHV-6B[5], and KSHV[6], the herpesvirus capsid floor is characterized by either type I, II, or III MCP-MCP interactions (Extended Data Fig. 3e-l). Type I interaction is intra-capsomeric while type II and type III are inter-capsomeric. Types I, II, and III interactions are formed between two or three adjacent MCP subunits by either β-strands in the N-lasso, E-loop in the Johnson-fold and dimerization domains (Extended Data Fig. 3g,i-j), or α-helices in the dimerization domains (Extended Data Fig. 3h) of the neighboring MCPs. The lasso action (type III) occurs only between hexon-hexon MCPs (Extended Data Fig. 3i-j) but not penton-hexon MCPs (Extended Data Fig. 3k,l); this is due to the flexibility of the penton MCP N-terminus, which causes P6 MCP to refold into a conformation that effectively eliminates its lassoing ability (Extended Data Fig. 3k). Additionally, the inter-capsomeric interactions between α-helices in the dimerization domains (*i.e.*, type II) also only occur between hexon-hexon MCPs because the dimerization domain of penton MCP adopts a configuration which makes it unable to form type II interactions with the dimerization domain of P1 hexon MCP, rendering the P1 dimerization domain flexible (Extended Data Fig. 3k,l).

In contrast to these conserved MCP domain organization and MCP-MCP interaction schemes, the structures among individual MCP subunits of the capsid exhibit an unprecedented level of variability which we refer to as structural plasticity (Supplementary Video 8). We identified 20 unique conformations among the MCP structures resolved in each EBV capsid (Fig. 3; Extended Data Fig. 4): 16 within an icosahedral asymmetric triangle (Fig. 3e), 2 portal proximal (Extended Data Fig. 4a, right panel), and 2 related to CATC binding (Extended Data Fig. 4a, middle panel). These MCPs show structural plasticity at different degrees depending on their surroundings. 16 MCPs within the asymmetric unit vary in their local structures throughout multiple domains, particularly at their floor regions (Fig. 3e-p). Compared with P1, P6 and Pen MCPs, the structures of C1-C6, E1-E3, and P2-P5 MCPs do not have dramatic changes. The alignment of these 13 MCP models highlights not only the

1

conformational changes at their N-lasso domains (Fig. 3j) and two fragments (a.a. 124-172 and a.a. 1072-1091) in their Johnson-fold domains (Fig. 3k), but also the orientation switch (*i.e.*, being "up" and "down") of two MCP fragments (a.a. 1149-1169 and a.a. 1256-1267) in their buttress domains (Fig. 3h,i). Each triplex adopts a unique direction, but still can be stabilized by interacting with three quasi-equivalent neighboring MCPs. Different interacting sites on the heterotrimeric triplexes (Supplementary Figs. 4-5) might be responsible for the multiple binding states found in the buttress sub-domains (Fig. 3h,i).

Variations among MCP subunits can be observed in the floor regions of P1, P6 and Pen MCPs, particularly in N-lasso (Fig. 3o) and dimerization (Fig. 3n) domains. N-lasso of P1 MCP folds similarly with that of C1 MCP, but is completely different from those of P6 and Pen MCPs (Fig. 3o). Likewise, the fragment of a.a. 295-374 of P6 MCP folds in conformity with that of C1 MCP while differing vastly compared with those of P1 and Pen MCPs (Fig. 3n). It is worth noting that the fragment a.a. 1277-1323 in the buttress domain of Pen MCP folds into a long helix instead of two short helices in those of other 15 MCPs (Fig. 3m). As shown in Fig. 3p, the spine helix in the Johnson-fold domain of Pen MCP tilts downward ~40⁰ compared with the 15 hexon MCPs.

There are also variations in the P1 (and P6) MCP structures in the CATC-absent vertex (Extended Data Fig. 4a, left panel), CATC-binding vertex (Extended Data Fig. 4a, middle panel), and portal vertex (Extended Data Fig. 4a, right panel). Among these three, the portal vertex displays the greatest level of structural plasticity (P1 in Extended Data Fig. 4b-e; P6 in Extended Data Fig. 4f,g). Such structural variations may result from differences in capsid-bindings by CATC and portal proteins. For instance, fragment a.a. 80-96 of P1 MCP in the portal vertex flips up rather than down as those in the P1 MCPs of CATC-absent and CATC-binding vertices (Extended Data Fig. 4d). Fragments of a.a. 305-340 and a.a. 1146-1168 are missing in P1 MCP (Extended Data Fig. 4c,e) while a.a. 26-63 is invisible in P6 MCP (Extended Data Fig. 4g) in the portal vertex reconstruction. These variations in hexons MCPs, particularly P1 and P6 MCPs, and penton MCP reveal the intrinsic plasticity of MCP structure in EBV; the folding of individual domains is preserved with gradual structural changes spreading out across

different domains, rather than through an abrupt large-scale conformational switch (Fig. 3e-p). Despite remaining consistent with its role in organizing the three types of MCP-MCP interactions (Extended Data Fig. 3e-l), the greatest structural changes were observed in N-lasso areas. Taken together, the 20 unique conformers of MCP—16 MCPs within an asymmetric unit, 2 P1 and 2 P6 MCPs in CATC-binding penton and portal vertexes—unveil a remarkable level of structural plasticity of MCP not previously reported for any herpesviruses.
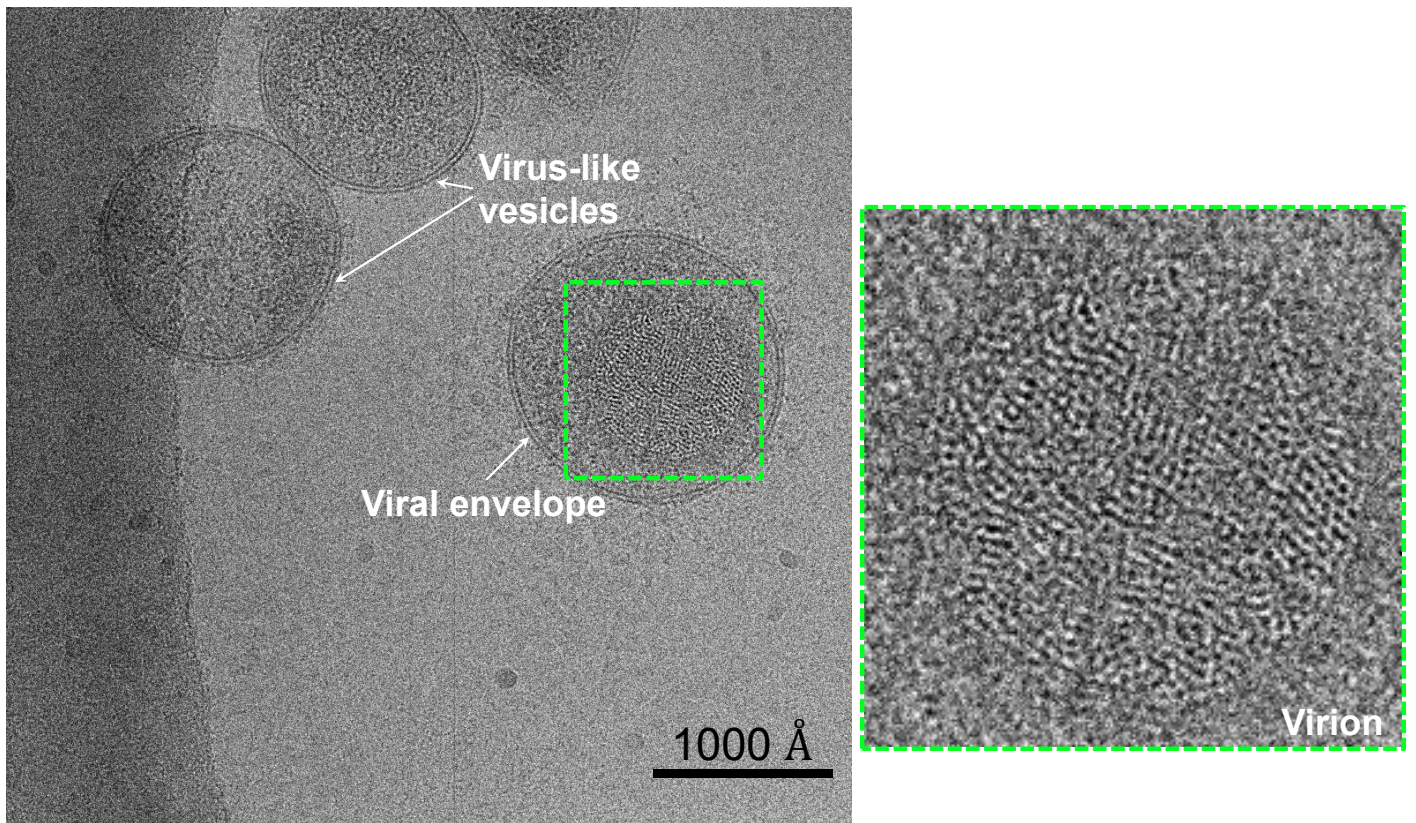
Supplementary Tables

Supplementary Table 1. Statistics of cryoEM imaging, data processing and model refinement.

Supplementary Table 2. Model building statistics.

Supplementary Table 3. RMSD statistics for MCP and Tri1.

References

1. Yu, X., Jih, J., Jiang, J. & Zhou, Z.H. Atomic structure of the human cytomegalovirus capsid with its securing tegument layer of pp150. *Science* **356**, eaam6892 (2017).
2. Dai, X. & Zhou, Z.H. Structure of the herpes simplex virus 1 capsid with associated tegument protein complexes. *Science* **360**(2018).
3. Wang, J. et al. Structure of the herpes simplex virus type 2 C-capsid with capsid-vertex-specific component. *Nature Communications* **9**, 3668 (2018).
4. Yuan, S. et al. Cryo-EM structure of a herpesvirus capsid at 3.1 Å. *Science* **360**(2018).
5. Zhang, Y. et al. Atomic structure of the human herpesvirus 6B capsid and capsid-associated tegument complexes. *Nature Communications* **10**, 5346 (2019).
6. Dai, X. et al. Structure and mutagenesis reveal essential capsid protein interactions for KSHV replication. *Nature* **553**, 521 (2018).
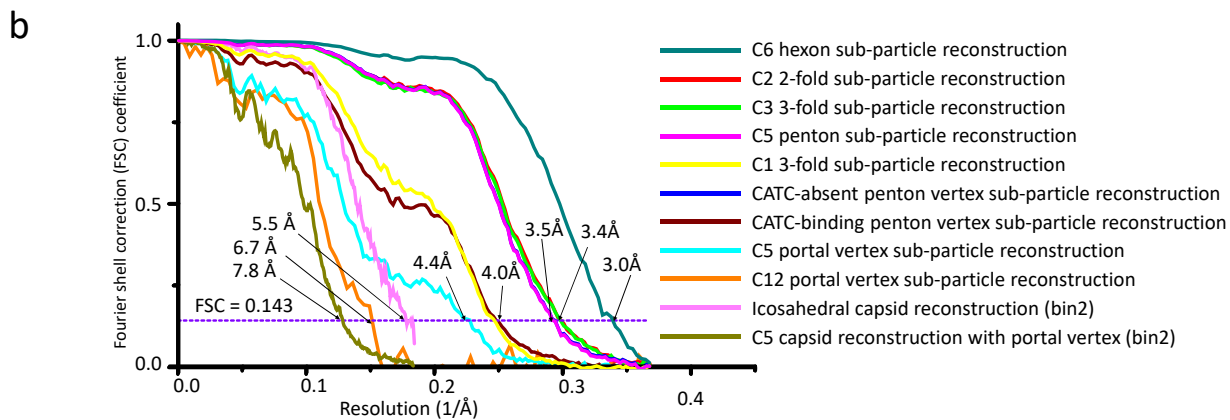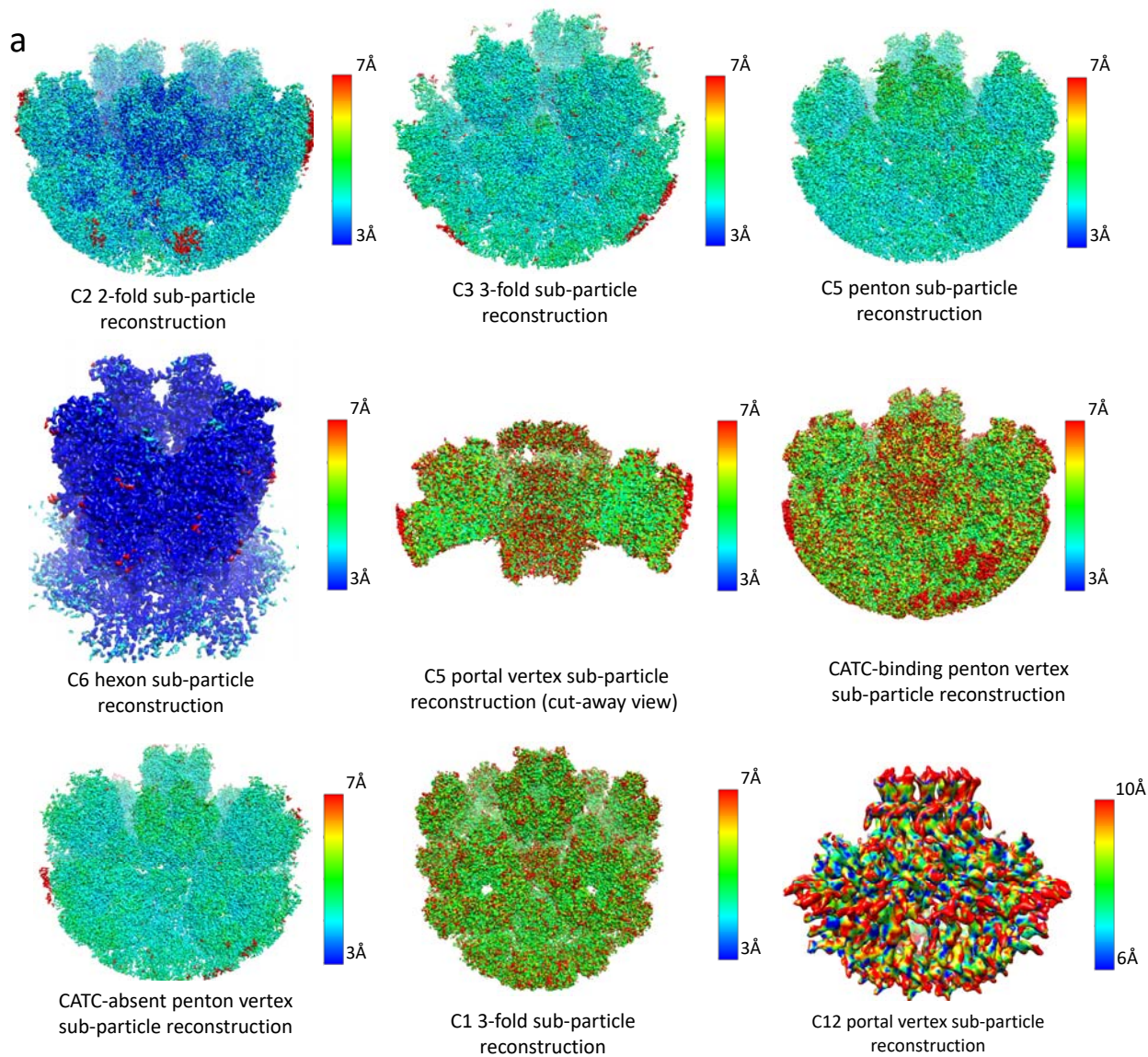
Supplementary Figure 1. A representative cryoEM micrograph containing one EBV virion particle. Two types of particles can be seen: virion containing a nucleocapsid (marked by a green box, middle) and virus-like vesicles[39] (upper left). Zoomed-in in the right panel is the nucleocapsid showing fingerprint-like pattern, characteristic of dsDNA.
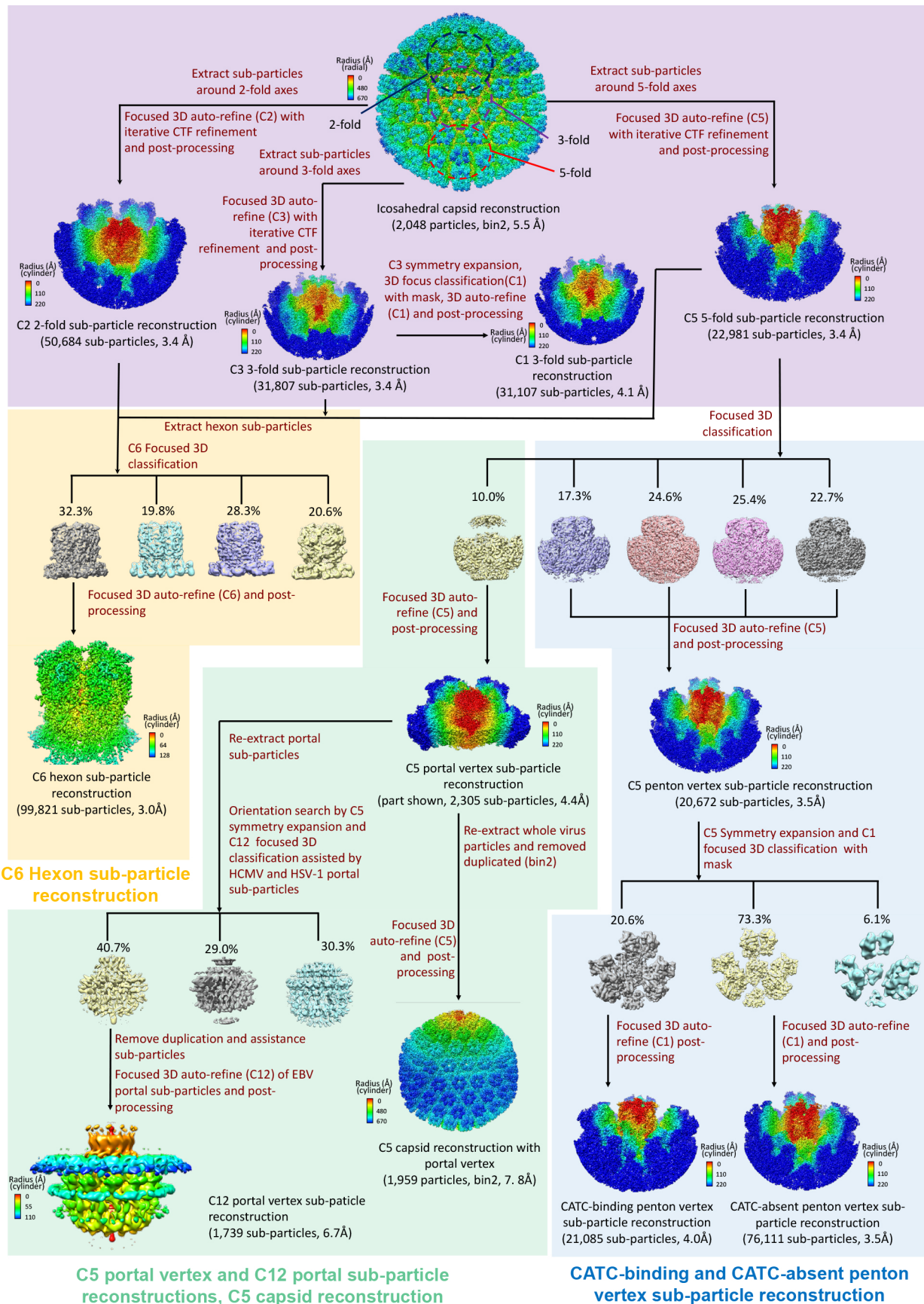
Supplementary Figure 2. Data processing workflow for sequential symmetry relaxation sub-particle reconstruction. Red texts next to arrows describe the processing steps; black texts describe the properties of the data or the result of the respective steps. Color shade groups steps used for the same (or similar as in the main-axis sub-particles) type of sub-particle reconstructions.

Supplementary Figure 3. **Resolution assessment of 3D reconstructions.** (**A**) Local resolution evaluation of sub-particle reconstructions by ResMap[59]. Color bar represents resolution range. (**B**) "Gold-standard" Fourier shell correlation (FSC) curves of the 3D reconstructions. The resolutions of the icosahedral reconstruction and C5 whole virus reconstruction are 5.6 Å and 7.8 Å, respectively; those for the other sub-particles are as follow: 3.0 Å (C6 hexon sub-particle reconstruction), 3.4 Å (C2 2-fold sub-particle reconstruction), 3.4 Å (C3 3-fold sub-particle reconstruction), 3.5 Å (C5 penton vertex sub-particle reconstruction), 4.0 Å (CATC-binding sub-particles reconstruction), 4.1 Å (C1 3-fold sub-particles reconstruction), 3.5 Å (CATC-absent penton sub-particle reconstruction) and 4.4 Å (C5 portal vertex sub-particles reconstruction). All resolutions are based on the 0.143 FSC criterion [51].
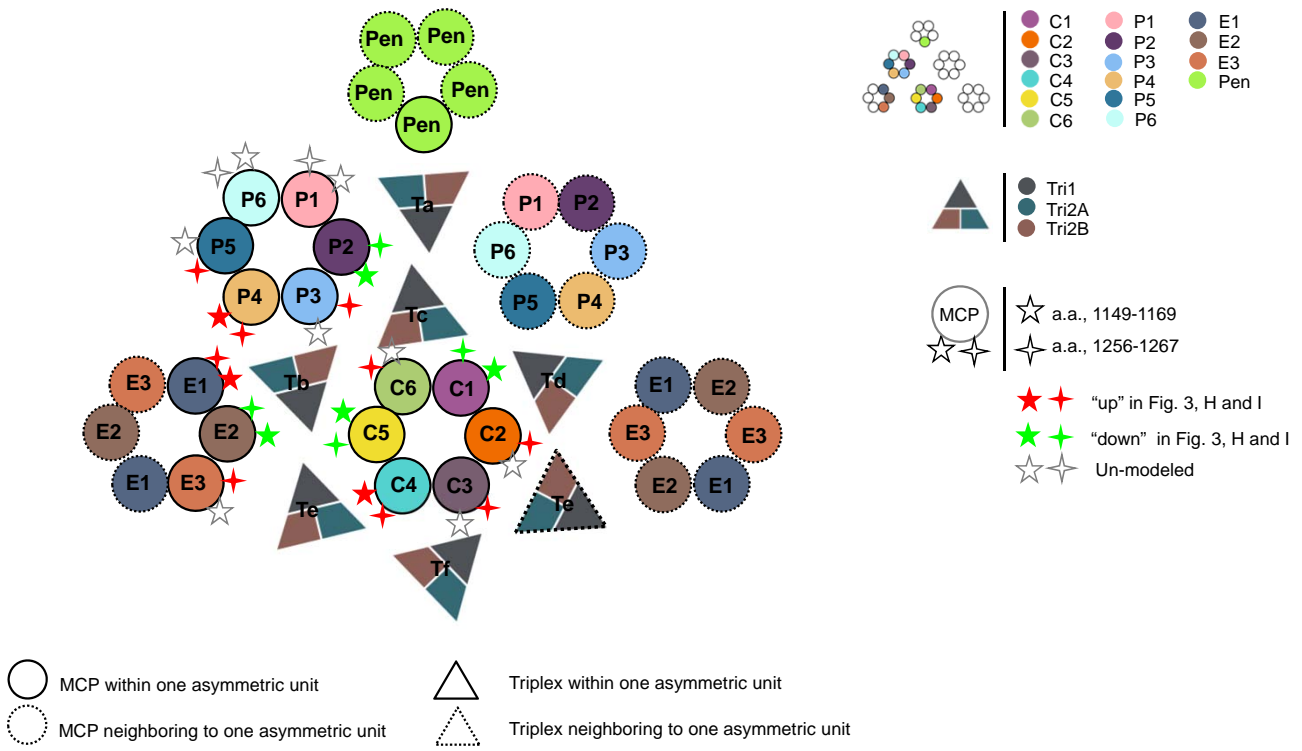
Supplementary Figure 4. Schematic diagram of plasticity of triplex interactions with MCP buttress domain shown in Figure 3h,i.
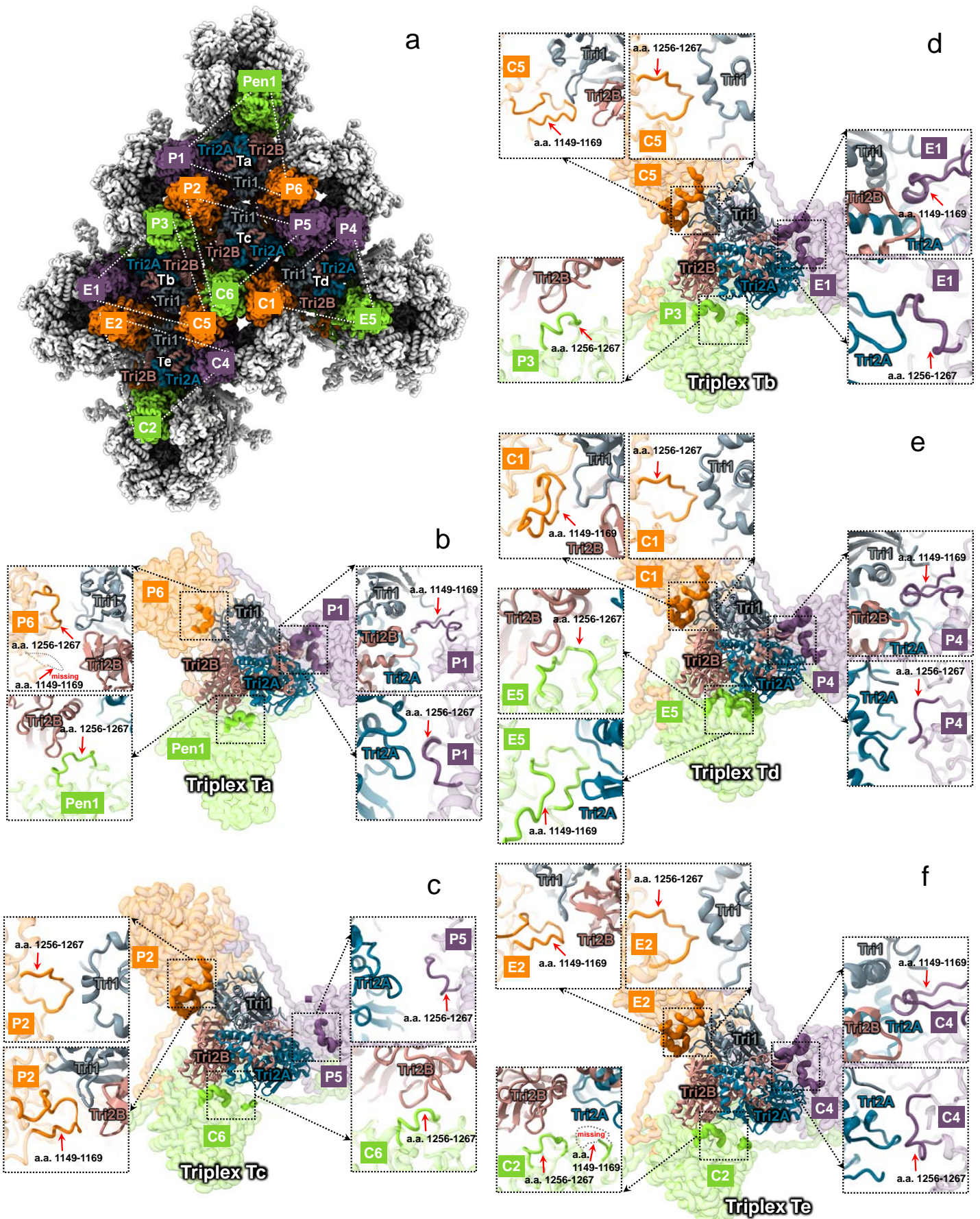
Supplementary Figure 5. **Details of plasticity of triplex interactions with MCP buttress domain shown in Figure 3h,i.** (**A**) Distribution of triplexes Ta, Tb, Tc, Td, and Te in the MCP network. (**B-F**) Magnified profile views of the regions surrounding triplexes Ta (B), Tb (D), Tc (C), Td (E), and Te (F) as viewed from the outside of the capsid. Away from the capsid floor, triplex Ta is dominantly stabilized by two long loop-containing segments (*a.a.* 1149-1169 and *a.a.* 1256-1267) from the buttress domains of P1 MCP (purple), P6 MCP (orange), and Pen1 MCP (green) (B). Tb (D), Tc (C), Td (E), and Te (F) triplexes are stabilized by their surrounding MCPs in an architecturally similar but locally different manner.